ACS Catalysis

Research Article

pubs.acs.org/acscatalysis

Tuning Catalytic Selectivity: Zeolite- and Magnesium Oxide-Supported Molecular Rhodium Catalysts for Hydrogenation of 1,3-Butadiene

Dicle Yardimci, Pedro Serna,* and Bruce C. Gates*

†Department of Chemical Engineering and Materials Science, University of California, Davis, One Shields Avenue, Davis, California 95616, United States

Supporting Information

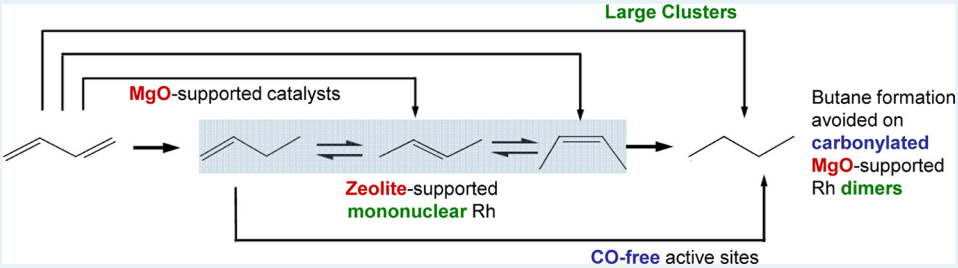

ABSTRACT: Regulation of the catalytic selectivity of rhodium for the industrially important hydrogenation of 1,3-butadiene to *n*-butenes has been achieved by controlling the structure of essentially molecular rhodium species bound to supports. The selectivity for *n*-butene formation increases as the nuclearity of the metal species decreases from several Rh atoms to one, but these catalysts form the undesired product *n*-butane, even at low diene conversions. The *n*-butene selectivity increases when the rhodium is selectively poisoned with CO ligands, and it is highest when the support is the electron-donor MgO and the rhodium is in the form of clusters that are well approximated as dimers. The electron-donor support is crucial for stabilization of the rhodium carbonyl dimer sites, as it limits the oxidative fragmentation of the clusters—which is facilitated when the support is HY zeolite (a poor electron donor)—that leads to decreased catalytic activity and selectivity. The selective MgO-supported rhodium carbonyl dimers suppress the catalytic routes that yield butane, limiting the activity for H_2 dissociation to avoid butane formation via primary reactions and also favoring the bonding of 1,3-butadiene over butenes to limit secondary reactions giving butane. With this catalyst, selectivities to *n*-butene of >99% were achieved at 1,3-butadiene conversions as high as 97%. This selectivity matches that of any reported for this reaction, and the catalyst works under milder conditions (313 K and 1 bar) than others that are selective for this reaction.

KEYWORDS: *1,3-butadiene, supported rhodium catalyst, catalyst selectivity, molecular catalyst, selective hydrogenation*

INTRODUCTION

1,3-Butadiene is a byproduct in the manufacture of butenes by thermal cracking of petroleum fractions, and when the butene is subsequently converted, this diene must be removed because it (a) leads to side products that reduce product quality and (b) causes deactivation of the catalysts used to manufacture either polymers from 1-butene or high-octane-number gasoline components from isobutylene. Thus, researchers have been motivated to discover active, selective catalysts to convert 1,3-butadiene to butenes in the presence of excess butenes.

The literature of selective 1,3-butadiene hydrogenation shows that catalysts can be ranked approximately in terms of decreasing selectivity, as follows: gold > palladium ≫ platinum ∼ rhodium.[1−3] The catalytic performance of palladium, platinum, and rhodium in the form of particles large enough to be metallic has been assessed in terms of the modes of adsorption of 1,3-butadiene and butenes.[2−5] In contrast, little is known about the action of highly dispersed supported catalysts that incorporate only a few metal atoms. Gold in such a form is active for this and other hydrogenation reactions,[6−8] and it is highly selective for the formation of *n*-butenes.[1] Nonetheless, the best gold catalysts are much less active than supported palladium, platinum, or rhodium. Thus, researchers are motivated to discover improved catalysts that are highly active and selective for 1,3-butadiene hydrogenation.

Here, we report such a catalyst. It consists of nearly uniform, essentially molecular, dimeric rhodium sites on a solid support. This discovery was guided by the following principles: supported catalysts consisting of highly uniform sites incorporating, at most, a few metal atoms are (a) essentially molecular in character, lending themselves to precise structural elucidation; (b) tunable by choice of the ligands, as in solution organometallic catalysis, with the support being ligands; and (c)

Received: July 16, 2012
Revised: August 20, 2012
Published: August 22, 2012

potentially selective because of the uniformity of the catalytic species.

We investigated rhodium catalysts, because, although rhodium is highly active in various forms for hydrogenation,[9−11] rhodium has been little explored for diene hydrogenation, possibly because, like other noble metals in the form of supported clusters or particles, it is unselective for butenes. We postulated that new catalytic chemistry of rhodium could emerge if the catalytic species were essentially molecular so that they could be tuned by the choice of the metal nuclearity and ligands. Thus, we investigated the influence of the following catalyst design variables on the activity and selectivity of supported rhodium for 1,3-butadiene hydrogenation: (a) the metal nuclearity, ranging from one to several; (b) the electron-donor properties of the support; and (c) other ligands on the rhodium, including reactive hydrocarbons and CO.

Molecular-scale control of the catalytic species was guided by reports[12] indicating how the metal precursor, support, and reactive atmosphere allow regulation of the structure of the catalytic species. The catalyst structures were investigated with infrared (IR), X-ray absorption near edge structure (XANES), and extended X-ray absorption fine structure (EXAFS) spectroscopies. Catalyst performance was evaluated on the basis of (a) the activity (measured as a turnover frequency, TOF, [molecules of 1,3-butadiene converted] × [Rh atom × s]$^{-1}$; (b) the selectivity at various 1,3-butadiene conversions; and (c) the changes in performance as a function of time on stream in a flow reactor.

The results demonstrate striking differences in the catalytic chemistry of rhodium as a function of the structure and composition of the catalytically active species, and we interpret them in terms of differences in the interactions between the reactants (1,3-butadiene and H_2) and these species. The structure of the catalyst was precisely tuned to suppress the catalytic routes yielding butane, both in primary and secondary reactions. Tuning of the catalyst structure involved conversion of monorhodium species to dimers and selective poisoning with CO. Thus, we report a supported dimeric rhodium catalyst that, in contrast to the reported catalysts,[3,4] is highly active and selective for the hydrogenation of 1,3-butadiene to butenes.

RESULTS

Synthesis and Structural Characterization of Supported Catalysts. $Rh(C_2H_4)_2(acac)$ (acac is acetylacetonate) was used as a catalyst precursor. MgO- and zeolite-supported rhodium complex catalysts were synthesized by slurrying the precursor with either support in *n*-pentane at 298 K and 1 bar for 24 h, followed by evacuation to remove the solvent.[13] The MgO- and HY zeolite-supported catalysts contained 0.4 and 1 wt % rhodium, respectively. The rhodium loadings were chosen to be high enough to give satisfactory signal-to-noise ratios in the EXAFS spectra and to be low enough to ensure a wide average spacing of the surface sites with the goal of site isolation and uniformity.[14]

Contacting of $Rh(C_2H_4)_2(acac)$ with each support led to chemisorption to give the supported mononuclear complex $Rh(C_2H_4)_2$, as shown by the IR and EXAFS spectra (Figures in Supporting Information (SI), S1 and S2, and Table 1). Details of the analysis of the spectra are provided in the SI. The EXAFS spectra show that $Rh(C_2H_4)_2$ on each support was anchored by two Rh−O bonds; thus, these species were isostructural.[13,15]

Table 1. EXAFS Fit Parameters[a] Characterizing MgO-Supported Rhodium-Containing Species at the Rh K edge[b]

sample	shell	*N*	*R* (Å)	$10^3 \times \Delta\sigma^2$ (Å^2)	ΔE_0 (eV)
1	Rh−Rh				
	Rh−C_{ethene}	4.0	2.06	1.3	2.7
	Rh−$O_{support}$	2.2	2.15	1.8	−5.1
	Rh−Mg	1.2	3.09	3.5	3.8
2	Rh−Rh				
	Rh−C_{ethene}	3.7	2.08	3.8	3.8
	Rh−$O_{support}$	2.1	2.15	3.1	7.1
	Rh−Al	1.1	3.02	6.7	−2.5
3	Rh−Rh	1.0	2.71	5.8	−2.9
	Rh−C_{ethyl}	1.2	2.09	0.01	6.9
	Rh−$O_{support}$	1.0	2.21	2.7	7.2
	Rh−Mg	0.7	2.86	0.07	0.6
4	Rh−Rh	2.8	2.69	10.5	3.8
	Rh−$O_{support}$	0.5	2.20	6.8	−2.6
	Rh−Al	0.5	3.00	2.1	−7.0
5	Rh−Rh	1.0	2.73	4.7	1.1
	Rh−$C_{COterminal}$	1.8	1.83	1.4	7.9
	Rh−$O_{COterminal}$	1.8	3.04	9.3	−7.5
	Rh−$C_{CObridging}$	2.1	1.97	0.35	7.9
	Rh−$O_{CObridging}$	2.5	3.22	3.7	7.9
	Rh−$O_{support}$	1.0	2.08	1.0	7.5
6	Rh−Rh	0.3	2.73	1.62	3.8
	Rh−$C_{COterminal}$	1.5	1.84	4.8	7.8
	Rh−$O_{COterminal}$	1.5	3.06	8.3	−7.4
	Rh−$O_{support}$	1.9	2.17	12	−7.0
	Rh−Al	0.5	3.22	0.01	3.5
7	Rh−Rh	0.8	2.70	5.5	5.5
	Rh−$C_{COterminal}$	2.0	1.88	8.5	8.0
	Rh−$O_{COterminal}$	2.0	2.98	12	−5.3
	Rh−$O_{support}$	2.0	2.03	4.0	4.7
	Rh−$C_{Hydrocarbon}$				
	Rh−Mg	1.4	3.03	3.3	7.9

[a]Notation: *N*, coordination number; *R*, distance between absorber and backscatterer atoms; $\Delta\sigma^2$, disorder term; ΔE_0, inner potential correction. Error bounds (accuracies) characterizing the structural parameters obtained by EXAFS spectroscopy are estimated to be as follows: *N*, ±20%; *R*, ±0.02 Å; $\Delta\sigma^2$, ±20%; and ΔE_0, ±20. [b]Sample 1, formed from adsorption of $Rh(C_2H_4)_2(acac)$ on MgO (Δk = 3.8−13.3 Å^{-1}, Δr = 0.8−3.7 Å). Sample 2, formed by adsorption of $Rh(C_2H_4)_2(acac)$ on zeolite HY (Δk = 3.7−12.8 Å^{-1}, Δr = 0.8−3.8 Å). Sample 3 is sample 1 after treatment with continuously flowing H_2 at 353 K for 1 h (Δk = 3.33−11.70 Å^{-1}, ΔR = 0.8−4.0 Å). Sample 4 is sample 2 after treatment with continuously flowing H_2 at 353 K for 1 h (Δk = 3.27−13.66 Å^{-1}, Δr = 0.8−4.0 Å). Sample 5 is sample 3 after treatment with a pulse of CO at 298 K and 1 bar (Δk = 3.11−13.92 Å^{-1}, ΔR = 0.8−4.0 Å). Sample 6 is sample 4 after treatment with a pulse of CO at 298 K and 1 bar (Δk = 3.17−14.84 Å^{-1}, ΔR = 0.8−4.0 Å). Sample 7 is sample 5 after treatment in flowing 1,3-butadiene and H_2 at 313 K and 1 bar for 20 h (Δk = 2.95−14.12 Å^{-1}, Δr = 0.8−4.0 Å).

Transformation of the supported rhodium complexes into extremely small clusters resulted from treatment in flowing H_2 at 353 K and 1 bar;[16,17] when the support was MgO, the ethylene ligands π-bonded to the rhodium reacted relatively slowly to give ethane and butane (detected with an online mass spectrometer) as well as σ-bonded ethyl ligands. These changes were evidenced by IR spectra showing a gradual decrease in intensity of the bands characterizing the CH_2 moiety of the ethylene ligands, at 3059 and 2999 cm^{-1}, and a concomitant increase in intensity of the bands at 2963, 2924, and 2880 cm^{-1},

dx.doi.org/10.1021/cs300475c | ACS Catal. 2012, 2, 2100−2113

characterizing the CH_3 groups of ethyl ligands[15] (SI Figure S3). In contrast, when the support was the zeolite, the change was rapid, giving exclusively the fully hydrogenated compounds, as the decrease of the ethylene bands at 3060 and 3016 cm^{-1}[13] was not accompanied by an increase of the bands characteristic of CH_3 groups (SI Figure S4).

The EXAFS data are consistent with the IR and mass spectrometric results characterizing the H_2-treated samples (Table 1). When the support was MgO, they show a decrease in the Rh−C first-shell coordination number from ∼4 prior to the treatment to ∼1. When the support was the zeolite, the Rh−C first-shell coordination number became undetectable. Thus, we infer that the initial ethylene ligands on the MgO-supported rhodium complexes were converted into ethyl ligands, ethane, and butane, whereas only gas-phase alkanes formed as hydrocarbon products when the support was the zeolite.

These changes in the ligands were accompanied by (a) a decrease of the white line intensity in the XANES spectra (SI Figure S5), indicating reduction of the rhodium;[16,17] (b) a decrease in the Rh−O coordination number (from ∼2 to ∼1 when the support was MgO and to ∼0.5 when it was the zeolite; Table 1), indicating a decrease in the number of metal−support bonds;[16] and (c) the appearance of a new contribution at a relatively long Rh−backscatterer distance indicative of Rh−Rh bonds (Table 1).

When the support was MgO, the H_2 treatment led to the formation of sites consisting, on average, of only two Rh atoms each (characterized by a Rh−Rh coordination number of ∼1 at a bonding distance of ∼2.71 Å). In contrast, when the support was the zeolite, the clusters that formed consisted of ∼4 Rh atoms each on average (characterized by a Rh−Rh coordination number of ∼3 at a bonding distance of ∼2.69 Å), in agreement with previous reports.[16,18] The higher nuclearity of the clusters formed on the zeolite is consistent with the results (vide supra) showing a more significant attenuation of the Rh−C and Rh−O contributions characterizing the interaction of the metal with the alkyl ligands and with the support, respectively, when the support was the zeolite. The presence of isosbestic points in the time-resolved XANES spectra of the MgO-supported sample during the H_2 treatment, but not the zeolite-supported sample (SI Figure S5), indicates a stoichiometric transformation of one species into another on the MgO but the formation of a mixture of rhodium species on the zeolite.[19]

When each of the samples (mononuclear rhodium complexes and rhodium clusters on each support) was treated with a pulse of CO in flowing helium at 298 K and 1 bar (350 CO molecules per Rh atom), carbonylation of the rhodium occurred within 2 min,[15,17,18] as shown by the IR spectra (Figure 1).

The appearance of two relatively sharp ν_{CO} bands in the IR spectra of the unreduced MgO- and zeolite-supported samples (Figure 1), at 2000 and 2074 cm^{-1}, and 2053 and 2118 cm^{-1}, respectively, confirms the presence of mononuclear rhodium *gem*-dicarbonyls, and these were the only form of rhodium on either support.[15,17] The marked blue shift of the ν_{CO} bands characterizing the zeolite-supported sample indicates that the rhodium on that support was electron-deficient, more so than that on MgO, consistent with the fact that MgO is a better electron donor than the zeolite.[20]

The samples that had been reduced in H_2 prior to exposure to CO were characterized by IR bands that indicate rhodium carbonyls in addition to the mononuclear rhodium *gem*-dicarbonyls. The MgO-supported sample was characterized by multiple new bands in the ν_{CO} region, at 2074, 2025, 2001, 1958, 1893, and 1853 cm^{-1}, the latter two being sharp and intense, corresponding to CO ligands bridging two Rh atoms and therefore characteristic of rhodium clusters.[21−23] The spectra of these supported rhodium carbonyl clusters (Figure 1A) are markedly different from those of well-known clusters, such as $Rh_4(CO)_{12}$, $Rh_6(CO)_{16}$, $[Rh_5(CO)_{15}]^-$, and $[Rh_{12}(CO)_{30}]^{2-}$,[15,24,25] instead strongly resembling those assigned to partially carbonylated rhodium dimers.[26] A more complete interpretation of the spectra is presented in the SI.

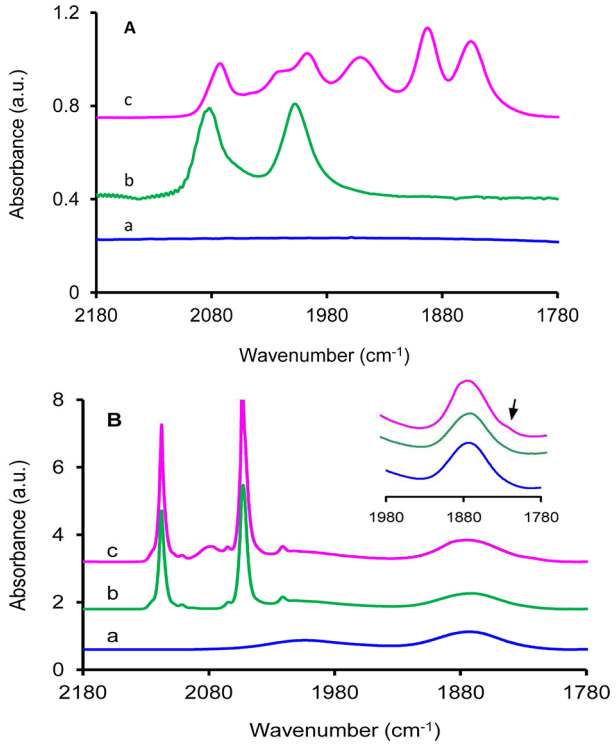

Figure 1. IR spectra characterizing the CO stretching region of MgO-supported catalysts (A) and zeolite HY-supported catalysts (B) treated in the following sequence: in helium at 298 K and 1 bar after chemisorption of $Rh(C_2H_4)_2(acac)$ on the supports (a); the preceding samples after exposure to a pulse of CO in helium at 298 K and 1 bar (b); samples (a) after treatment in H_2 at 353 K and 1 bar for 1 h, and treated with a pulse of CO in helium at 298 K and 1 bar (c).

In agreement with the IR spectra, the EXAFS spectra of the MgO-supported rhodium carbonyl dimers show that the Rh−Rh contribution remained unchanged as a result of the CO exposure, although the spectra indicate changes in the rhodium ligation. The Rh−O distances indicate two different types of rhodium carbonyls (Table 1), each with a coordination number of ∼2. The carbonyl ligands are characterized by a total Rh−CO coordination number of ∼4, with each rhodium bonded to approximately two terminal carbonyls (four terminal ligands per rhodium dimer), bridged by two other CO ligands (two bridging ligands per rhodium dimer, shared by the two rhodium atoms in the site). The partially carbonylated rhodium dimers are thus approximated as $Rh_2(CO)_4(\mu\text{-}CO)_2$ species (from here on, referred to simply as $Rh_2(CO)_6$), each bonded to the support by two Rh−O bonds. These EXAFS results are consistent with the IR spectra demonstrating the presence of both terminal and bridging CO ligands.

dx.doi.org/10.1021/cs300475c | *ACS Catal.* 2012, 2, 2100−2113

Table 2. Summary of Structural Data and Catalytic Performance Data Characterizing Mononuclear Rhodium Complexes and Rhodium Clusters Supported on DAY Zeolite and on MgO (feed composition: 2 vol % 1,3-butadiene, balanced with H_2; total pressure =1 bar)

							distribution of *n*-butenes (%)		
catalyst	support	Rh−Rh coordination number determined by EXAFS data[a]	ligands bonded to rhodium determined by IR and EXAFS data	reaction temperature (K)	catalytic activity for 1,3- butadiene hydrogenation TOF (s^{-1})[b]	selectivity to *n*-butenes (%)	1-butene	*trans*-2-butene	*cis*-2-butene
(a), sample formed from $Rh(C_2H_4)_2(acac)$ adsorbed on MgO	MgO	n.d.[c]	C_2H_4	313	0.007	91.5	53.6	34.6	11.8
(b), sample formed from $Rh(C_2H_4)_2(acac)$ adsorbed on HY zeolite	zeolite HY	n.d.[c]	C_2H_4	313	0.014	92.5	23.4	10.7	65.9
(c), sample (a) treated with a CO pulse in helium at 298 K	MgO	n.d.[c]	CO	313	<0.0001				
(d), sample (b) treated with a CO pulse in helium at 298 K	zeolite HY	n.d.[c]	CO	313	0.0008	94.6	18.6	6.1	75.3
(e), sample (a) treated with H_2 at 353 K for 1 h	MgO	1.0 ± 0.2	C_2H_5	298	0.14	82.4	55.4	33.7	10.8
(f), sample (b) treated with H_2 at 353 K for 1 h	zeolite HY	2.8 ± 0.6	n.d.[c]	298	0.18	43.1	44.9	28.1	27.0
(g), sample (e) treated with a CO pulse in helium at 298 K	MgO	1.0 ± 0.2	CO	313	>0.05	>99	51.3	38.9	9.8

[a]The complete set of parameters determined in the EXAFS data fitting are provided in Table 1. [b]Turnover frequency: [molecules of 1,3-butadiene converted] × [Rh atom × s]$^{-1}$; calculated from differential conversions at time on stream = 0 (extrapolated from the corresponding conversion vs time on stream curves), assuming that that all Rh atoms were accessible to reactants. [c]Not detected.

The spectra show a strong support dependence (Figure 1). In contrast to the MgO-supported sample, the H_2-treated zeolite-supported sample after exposure to CO is characterized by an IR spectrum different from that of the mononuclear rhodium *gem*-dicarbonyl on the zeolite, but only by the presence of two weak, broad bands, at 2081 and 1830 cm^{-1} (Figure 1), the latter (partially masked by a band characteristic of the zeolite framework[27]) attributable to CO species bridging two Rh centers (and hence, to the presence of rhodium clusters).[28] However, the ratio of intensities of the bands assigned to rhodium *gem*-dicarbonyl species on the zeolite, at 2053 and 2118 cm^{-1}, to those at 2081 and 1830 cm^{-1}, is high, indicating the predominance of the mononuclear species over the clusters.

Thus, we infer that most of the clusters formed on the zeolite by treatment of the $Rh(C_2H_4)_2$ complexes with H_2 broke up as a result of the reaction with CO. Consistent with this inference, the EXAFS spectra of the catalyst after the CO exposure show that the Rh−Rh coordination number decreased from 2.8 to 0.3 (Table 1). The resulting supported species incorporated, on average, ∼1.5 CO ligands per Rh atom, consistent with a mixture of mononuclear $Rh(CO)_2$ species with a small fraction of rhodium carbonyl clusters. These results agree with the reported behavior of supported rhodium clusters undergoing oxidative fragmentation in CO when the support is acidic and the metal species are small (<1 nm in diameter).[29−32] The fact that the cluster fragmentation in the CO atmosphere was not complete is consistent with the XANES spectra (SI Figure S5), indicating that the reduced zeolite-supported sample consisted of a mixture of rhodium species.

The observation that the rhodium dimers on the electron-donor MgO are stable in the presence of CO is surprising because these dimeric species (a) do not break up, as do rhodium clusters on other metal oxide surfaces,[29−32] and (b) do not react to give the more stable tetranuclear or hexanuclear clusters, as is typically observed with unsupported rhodium carbonyl dimers at the low CO partial pressures used here.[23,30] The stabilization of the rhodium dimers by the MgO might explain, at least in part, the hindrance of further growth of the clusters during the H_2 treatment, consistent with the inference that the dirhodium species were tightly bonded to the support, in contrast to the bonding to the zeolite.

Catalytic Hydrogenation of 1,3-Butadiene. The MgO- and zeolite-supported mononuclear rhodium complexes and clusters, with and without CO ligands, were tested as catalysts for the hydrogenation of 1,3-butadiene in experiments with a conventional tubular plug-flow reactor with an online gas chromatograph for product analysis. In the following summary of the catalyst performance, data are lacking for any sample consisting of carbonylated rhodium clusters on the zeolite because, as summarized above, contact of the zeolite-supported rhodium clusters with CO led to fragmentation of the rhodium frame.

The activity of each catalyst was determined with a feed of 2.0 vol % 1,3-butadiene and 98 vol % H_2 by measuring reaction rates determined from differential conversions of the diene in the range <10%. Reaction rates are reported per Rh atom (i.e., as turnover frequencies, TOF), assuming that all the Rh atoms were accessible to the reactants. The TOF values were determined by extrapolation of the data to zero time on stream in the flow reactor to exclude effects of catalyst deactivation (although data are also reported for longer times on stream).

dx.doi.org/10.1021/cs300475c | ACS Catal. 2012, 2, 2100−2113

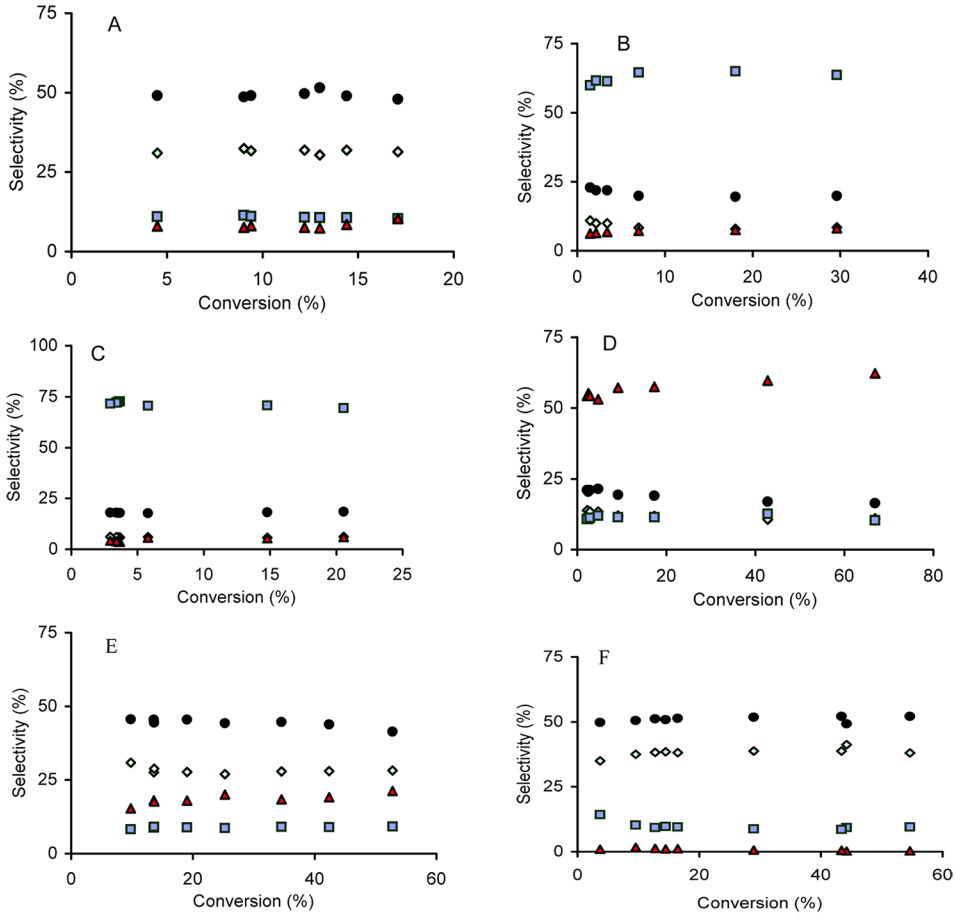

Figure 2. Selectivity plots characterizing catalysts in the following initial forms for the hydrogenation of 1,3-butadiene: (A) MgO-supported $Rh(C_2H_4)_2$ complexes, (B) zeolite-supported $Rh(C_2H_4)_2$ complexes, (C) zeolite-supported $Rh(CO)_2$ complexes, (D) zeolite-supported $Rh(C_2H_4)_2$ complexes after treatment at 353 K in H_2 for 1 h, (E) MgO-supported $Rh(C_2H_4)_2$ complexes after treatment at 353 K in H_2 for 1 h, and (F) MgO-supported $Rh(C_2H_4)_2$ complexes after treatment at 353 K in H_2 for 1 h and then treatment with a pulse of CO. ●, 1-Butene; green ◇, *trans*-2-butene; blue □, *cis*-2-butene; red △, butane. Reaction conditions are stated in Table 2.

Because there were substantial variations in activity from one catalyst to another, the catalyst testing was done at various temperatures to allow comparisons of selectivities at nearly constant conversions of at least 15% of the 1,3-butadiene. However, this conversion could not be reached with the MgO-supported $Rh(CO)_2$ catalyst, which was barely active in the range of temperatures investigated, 298−333 K, and unstable at higher temperatures because of rhodium cluster formation.

The catalyst performance data are summarized in Table 2, including selectivities to the butene isomers at a 1,3-butadiene conversion of 15%. This table also includes a summary of the structural characteristics of the catalysts inferred from the IR and EXAFS spectra.

The results of Table 2 led to the following comparison of the samples in terms of their hydrogenation activity: the $Rh(CO)_2$ complexes on each support were the least active species, and the rhodium clusters on each support were relatively high in activity, provided that they did not incorporate CO ligands. With regard to the selectivity for formation of *n*-butenes (at 15% 1,3-butadiene conversion), the CO-free rhodium clusters on each support were relatively unselective, with 82% of the products being *n*-butenes when the support was MgO, compared with only 43% when the support was the zeolite.

The striking result—and the major outcome of this work—is that the MgO-supported rhodium clusters approximated as dimers became highly selective catalysts when CO was incorporated as a ligand of the intact dimeric structure: the monoalkene selectivity was >99%. Preliminary results for this selective catalyst have been communicated.[18]

The catalysts also differ in the distribution of the *n*-butene isomers. The selectivity to 1-butene was always higher when MgO was the support (~53% of the butene, independent of the nuclearity and the ligand environment of the rhodium). When the support was the zeolite, the selectivity for formation of 1-butene was 45% of the butene when the rhodium was present as clusters, but only 19% when it was present as mononuclear complexes.

Selectivities were determined at various 1,3-butadiene conversions (the catalyst mass or the reactant flow rate, or both, were varied in these experiments) to provide a basis for identifying primary and nonprimary products (primary products include those formed directly from 1,3-butadiene, whereas higher-order products are formed in reactions involving readsorption of primary products). From the conversion versus selectivity curves determined for each catalyst (Figure 2), we have inferred the primary products, those showing clearly nonzero intercepts at zero conversion.[33]

The selectivity plot characterizing each of the catalysts (Figure 2) is markedly dependent on subtle changes in the

dx.doi.org/10.1021/cs300475c | *ACS Catal.* 2012, 2, 2100−2113

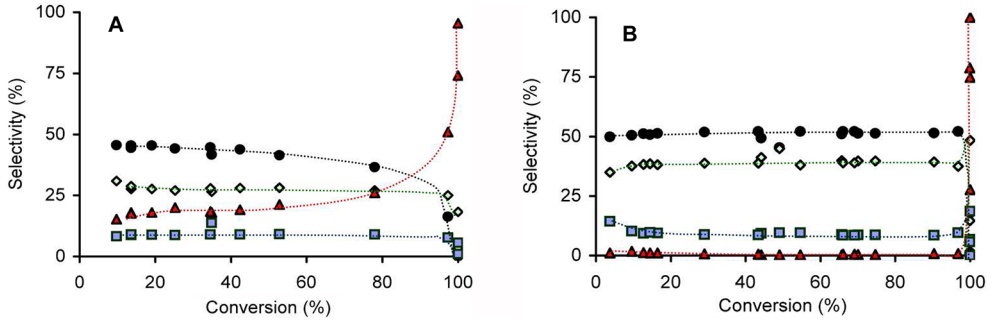

Figure 3. Selectivity plots for MgO-supported rhodium dimers in the absence (A) and in the presence (B) of CO ligands in the hydrogenation of 1,3-butadiene. ●, 1-Butene; green ◇, *trans*-2-butene; blue □, *cis*-2-butene; red △, butane. Reaction conditions are stated in Table 2.

nuclearity of the rhodium species, the support, and the ligands bonded to rhodium.

For example, butane, an undesired product in industrial practice, was formed as a primary product with a selectivity of 18% when the catalyst was MgO-supported rhodium dimers, as shown in Figure 2E. 1-Butene, *cis*-2-butene, and *trans*-2-butene also appear to be primary products formed on this catalyst (Figure 2E). As the conversion of 1,3-butadiene increased (Figure 3A), however, the selectivity to butane increased further, indicating that this product was additionally formed in secondary reactions (at 97% conversion, the overall selectivity to *n*-butenes had dropped to ~51%). Taking into account the observation that the increase in butane selectivity occurred as the selectivity to 1-butene decreased (Figure 3A), with the selectivity for formation of the 2-butenes constant for conversions up to 97%, we infer that the terminal alkene is a primary product, which may adsorb from the gas phase onto the catalytic sites to undergo further hydrogenation. In contrast, the other two butene isomers are primary products that do not undergo significant further reaction at 1,3-butadiene conversions <97% (but at higher conversions, the 2-butenes are also hydrogenated to butane, as shown in Figure 3A).

In contrast, all the primary and secondary routes that yield butane are suppressed on the MgO-supported rhodium dimers that incorporate CO ligands (Figure 3B), providing selectivities to *n*-butenes >99% at diene conversions as high as 97%, which is a striking result—that differentiates this catalyst not only from the others described here, but also from all the reported rhodium catalysts.[3,4]

The data also show that the performance of some of the catalysts changed during operation in the flow reactor. Particularly intriguing are the following observations: (a) the TOF characterizing the complex initially present as $Rh(C_2H_4)_2$ on MgO increased slightly with increasing time on stream, whereas that characterizing the isostructural rhodium complex on the zeolite decreased by almost 1 order of magnitude (Figure 4); (b) the decrease in activity with time on stream of the zeolite-supported sample initially present as $Rh(C_2H_4)_2$ was accompanied by a decrease in selectivity for *n*- butenes from ~93% to 82% (each determined at <15% 1,3-butadiene conversion), whereas the selectivity of each of the other samples (except for the $Rh(CO)_2$ complexes on the zeolite, for which a slight decrease was also observed) was essentially unchanged during operation (SI Figure S6); and (c) the activity of the MgO-supported rhodium species incorporating CO ligands increased markedly as a function of time on stream, provided that the metal was in the form of clusters, with

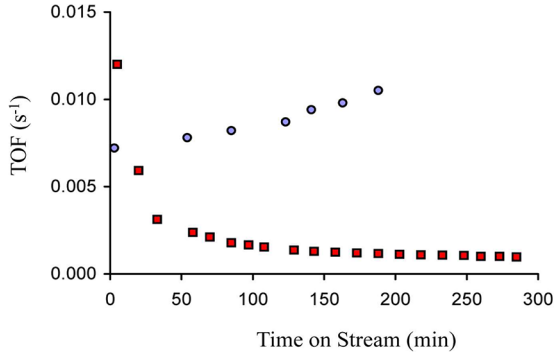

Figure 4. Evolution of TOF with time on stream characterizing MgO- (blue ○) and zeolite- (red □) supported catalysts initially in the form of $Rh(C_2H_4)_2$ complexes in the hydrogenation of 1,3-butadiene in a flow reactor. Reaction conditions are stated in Table 2.

conversions ranging from 1% at the beginning to 100% after several hours on stream (Figure 5A).

In attempts to understand the changes in catalyst performance during operation, we characterized the used catalysts by IR and/or EXAFS spectroscopies and also during operation in spectroscopic cells that were flow reactors. Mass spectrometry was used to determine the product compositions so that the catalyst performance could be related to the spectra. The results include IR spectra of the catalysts initially in the form of (a) MgO- and zeolite-supported $Rh(C_2H_4)_2$ (SI Figure S7), each before and after catalysis; (b) MgO-supported $Rh(CO)_2$ (SI Figure S8), before and after catalysis; and (c) carbonylated rhodium dimers during catalysis (Figure 5B). EXAFS data were also obtained characterizing the carbonylated rhodium dimers before and after catalysis. These spectra are discussed below.

Catalytic Activity for H−D Exchange in the Reaction of H_2 with D_2. Expecting that the dissociation of H_2 precedes hydrogenation of the C═C bonds in 1,3-butadiene, we investigated the reactivities of our catalysts for activation of H_2 by measuring the catalytic performance in the reaction of H_2 with D_2 to form HD. The catalysts tested in this reaction were MgO-supported rhodium complexes; MgO-supported rhodium dimers; zeolite-supported rhodium complexes; and zeolite-supported rhodium clusters, each in the absence of CO ligands.

In the H−D exchange reaction experiments, equimolar mixtures of H_2 + D_2 (diluted in helium and in the presence of small amounts, 0.45 vol %, of 1,3-butadiene) flowed through a bed of each catalyst in a tubular flow reactor operated at 298 K and 1 bar, with the concentration of HD in the product stream determined by mass spectrometry.

dx.doi.org/10.1021/cs300475c | *ACS Catal.* 2012, 2, 2100−2113

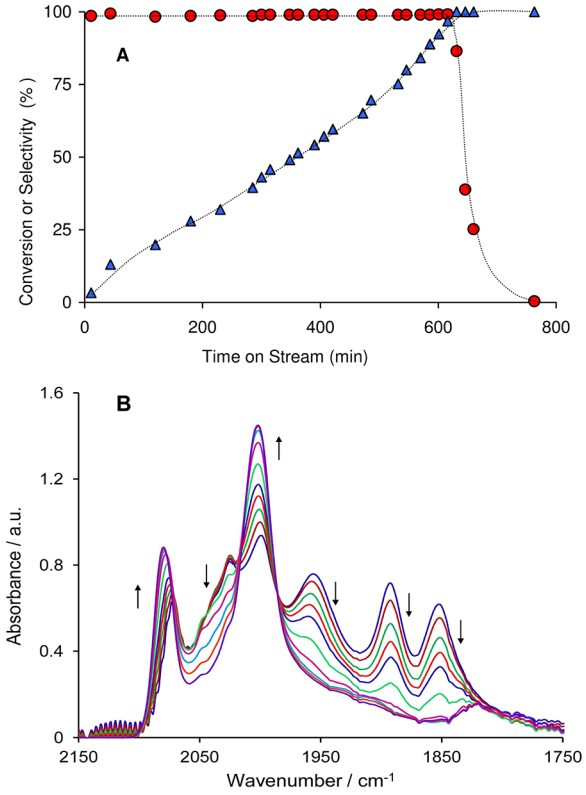

Figure 5. (A) Evolution of conversion (▲) and selectivity to *n*-butenes (○) in catalysis of 1,3-butadiene hydrogenation in a once-through flow reactor catalyzed by carbonylated rhodium clusters supported on MgO (reaction conditions: 313 K, 1 bar; total gas feed flow rate, 30 mL/min; feed component partial pressures, 20 mbar of C_4H_6, 980 mbar of H_2; mass of catalyst, 200 mg). (B) Time-resolved IR spectra of the MgO-supported rhodium carbonyl clusters in a flowing mixture of 1,3-butadiene and H_2 at 313 K and 1 bar.

The results (Figure 6) indicate that the catalysts incorporating rhodium species on the zeolite are more active for the

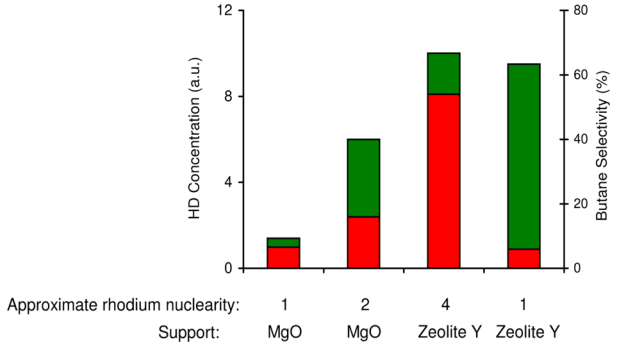

Figure 6. Concentration of HD species in exchange of H_2 and D_2 species (green bars) and selectivity to butane in the hydrogenation of 1,3-butadiene (red bars) on catalysts consisting of rhodium sites of various nuclearities on MgO and zeolite Y. The catalyst performance data are represented as HD concentrations in the product, stated in arbitrary units.

isotopic exchange reaction (and, we infer, for H_2 or D_2 dissociation)[34] than those supported on MgO. Furthermore, the results indicate that rhodium clusters on MgO are more active than the mononuclear rhodium complexes. CO caused a marked drop in activity for H−D exchange of each of our catalysts (SI Figure S10), a clear indication of the role of this ligand as a poison of the active sites.[35−37]

DISCUSSION

The 1,3-Butadiene Hydrogenation Reaction Network.

Earlier work[3] shows that 1,3-butadiene reacts with H_2 on transition metal surfaces according to one or more of the reaction pathways summarized in Scheme 1. In principle, each

Scheme 1. Reaction Pathways for the Hydrogenation of 1,3-Butadiene

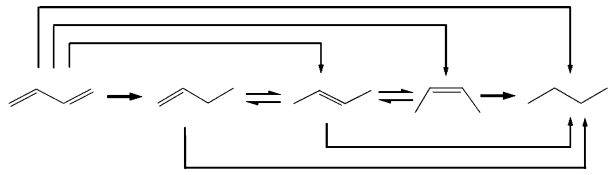

of the hydrogenation products (1-butene, *trans*-2-butene, *cis*-2-butene, and butane) can be formed in either primary or secondary reactions. The alkene isomerization is limited by equilibrium under our conditions (298−333 K, 1 bar), as follows: ∼60% *trans*-2-butene, ∼33% *cis*-2-butene, and ∼7% 1-butene.[38] (We neglect the skeletal isomerization to give isobutylene, because it was kinetically insignificant at our low temperatures.[39])

Among the reactions included in Scheme 1, the partial hydrogenation of 1,3-butadiene to give *n*-butenes, including 1-butene, which is the most valuable of the isomers for the manufacture of polymers,[40] is of great industrial interest, ideally requiring a catalyst that (a) does not simultaneously hydrogenate the two C═C bonds in the diene and (b) differentiates between the diene and the monoalkenes, preferentially activating the former even when the diene/monoalkene ratio is low. Thus, the ideal catalyst would limit the formation of butane as both a primary and a secondary product.

The performance of traditional palladium, platinum, and rhodium catalysts (in the form of extended metal surfaces or relatively large supported nanoparticles) is well understood on the basis of fundamental surface science.[2−5] For example, the generally higher selectivity of palladium relative to platinum for the formation of *n*-butenes has been attributed to differences in the adsorption modes of the diene; on palladium, 1,3-butadiene is di-π-bonded, but on platinum and on rhodium, it is di-σ-bonded.[3,4] The activation through a di-π-bonded species on palladium avoids the formation of butane as a primary product and, to a large extent, as a secondary product (as *n*-butene, activated via a di-σ-bonded species, competes unfavorably for the catalytic sites). Even so, the selectivities for formation of butenes on palladium drop drastically at high diene conversions because of readsorption of the monoalkenes when the 1,3-butadiene concentration is low.[41] Strategies for enhancement of the selectivity of palladium catalysts have been reported to have notable success.[41−44]

On rhodium and on platinum, in contrast, both the diene and the monoalkenes adsorb as di-σ-bonded species,[3,4] leading to the formation of butane as both a primary and a secondary product, resulting in low *n*-butene selectivities even at low diene conversions, a general characteristic of these catalysts.

The conventional palladium, platinum, and rhodium catalysts are all characterized by similar behavior with regard to the distribution of the *n*-butene isomers, as each is produced as a

dx.doi.org/10.1021/cs300475c | ACS Catal. 2012, 2, 2100−2113

primary product, with high selectivities to 1-butene observed when the diene conversion is low. This selectivity decreases as the 1,3-butadiene is increasingly consumed because the isomerization of the monoalkene becomes more significant. The *trans*-2-butene-to-*cis*-2-butene ratio is usually higher with palladium (∼13) than platinum or rhodium catalysts (<3).[3,4]

In the following sections, we evaluate the performance of our supported rhodium catalysts, which in contrast to those considered in the preceding paragraph are essentially molecular in character.

Hydrogenation of 1,3-Butadiene Catalyzed by Essentially Molecular Rhodium Species: Influence of the Metal Nuclearity and the Support. Our results for all but one catalyst are in line with the general observation that rhodium catalysts give significant yields of butane as a primary product in the 1,3-butadiene hydrogenation. Thus, our data show that butane is formed as a primary product (Figure 2), except when the conversion is catalyzed by the MgO-supported dimeric rhodium species incorporating CO ligands (discussed below). The formation of butane as a primary product suggests that the interaction between the diene and rhodium involves both of the diene C═C bonds and that both are converted before release of a product. This explanation accounts for the less than optimal selectivity to the desired *n*-butenes even at low diene conversions, as is typical of the reported rhodium catalysts.[3,4]

However, our results demonstrate that when the catalyst incorporates essentially molecular metal species, the selectivity can be controlled by subtle changes in the structure and composition of the catalytic sites, and these sites can be precisely characterized so that the catalytic properties can be unraveled. For example, the catalysts initially in the form of $Rh(C_2H_4)_2$ complexes on MgO and on HY zeolite produce *n*-butenes with ∼90% selectivity at low conversions (<15%, Table 1), whereas the catalysts incorporating rhodium clusters give significantly higher yields of butane (provided that CO is not present), with the selectivity depending on the rhodium cluster nuclearity. On MgO, with each catalytic site comprising only two Rh atoms, on average, the selectivity to the monoalkenes at low conversions is ∼84%, whereas on the zeolite, with each catalytic species consisting of clusters of 4 Rh atoms, on average, the selectivity is only about 57% at the same conversion (Table 1). Thus, the data show that the support plays a significant role in stabilizing the rhodium clusters, as the nuclearity of the clusters formed from the mononuclear rhodium complexes on MgO is lower than that of the clusters formed on the zeolite (Table 1). Furthermore, the data show that the cluster size affects the catalyst selectivity, with the fraction of the diene that is converted to butane via primary routes increasing as the nuclearity of the catalytic species increases.

To understand these results, one may consider that formation of butane as a primary product via two consecutive surface reaction steps would require that the hydrogenation of the second C═C bond (which requires activated species formed from H_2, presumably hydride) must be faster than the desorption of the butene intermediates. Thus, we infer that the selectivity for butane formation at low diene conversions should correlate with the activity of the catalyst for the activation of H_2, as determined in the H−D exchange reaction experiments. Indeed, among our catalysts, the selectivity for partial hydrogenation decreases as the activity for H−D exchange increases, corresponding to an increase in the nuclearity of the active sites from mononuclear rhodium to dirhodium to clusters with about 4 Rh atoms each. The relatively high activity of the rhodium clusters for the H−D exchange is consistent with the well-known role of neighboring noble metal centers for activation (dissociation) of H_2.[34,45,46]

In contrast, the mononuclear rhodium complexes on the zeolite (initially, $Rh(C_2H_4)_2$) do not fit this pattern, as they produce butane with selectivities similar to those provided by the isostructural species on MgO, but with a much higher activity for the activation of H_2 (Figure 6). Thus, although the selectivities to *n*-butenes provided by mononuclear rhodium complexes on MgO and on the zeolite are similar (∼ 90%), the reaction chemistry is strongly support-dependent. This comparison is explained as follows:

The fact that the zeolite-supported mononuclear species activate H_2 faster than the MgO-supported mononuclear species can be understood on the basis of the different electron-donor properties of the supports as ligands, as shown by the frequencies of the ν_{CO} bands characterizing the respective $Rh(CO)_2$ species (Figure 1) (the H_2 dissociation rate is higher when the metal is more electron-deficient (on the zeolite)).[14,17]

Notwithstanding the fast activation of H_2 by the zeolite-supported rhodium complexes, this catalyst is rather low in activity for the hydrogenation of alkenes (exemplified by ethylene),[17,47] a result that arises because the C═C bonds are activated not only by the mononuclear metal centers, but also by the acidic OH groups at the Al sites of the support neighboring the rhodium complexes, which favors fast formation of butenes via dimerization.[47] Neither oligomerization of the resulting butenes nor formation of butane by hydrogenation was observed.[47] Accordingly, we postulate that in the hydrogenation of 1,3-butadiene, the relatively low activity of these sites for the incorporation of dissociated hydrogen into *n*-butene accounts for the low yields of butane formed as a primary product, a result that could not have been anticipated on the basis of the correlation between the selectivity and the H−D exchange results obtained for the other catalysts (Figure 6).

Thus, the data show how the support plays a direct role in the catalytic hydrogenation of 1,3-butadiene. This point is assessed further below in an analysis of the distributions of *n*-butene isomers formed from 1,3-butadiene with each catalyst. On the electron-donor MgO, the mononuclear rhodium complexes initially present as $Rh(C_2H_4)_2$ lead to the formation of 1-butene as the main conformer (53% of the *n*-butene fraction), whereas the isostructural rhodium complexes on the HY zeolite give predominantly *cis*-2-butene (∼65% of the *n*-butene fraction), and these compositions do not match the equilibrium concentrations of the isomers under the reaction conditions ,whereby *trans*-2-butene would dominate.[38]

The high selectivity of the MgO-supported rhodium complexes for 1-butene formation indicates that (a) 1,2-hydrogen addition to 1,3-butadiene occurs preferentially over 1,4 addition[3,48,49] and (b) this catalyst isomerizes the terminal alkene at rates that are relatively low in comparison with those leading to its desorption from the catalyst.

In contrast, the formation of *cis*-2-butene catalyzed by closely similar species on the zeolite indicates that the rate of the isomerization reaction is boosted on this catalyst, a result that likely arises from the presence of the acidic sites on the support surface.[50] To explain the formation of a nonterminal butene as the major product on this catalyst (∼65% of the *n*-butene

dx.doi.org/10.1021/cs300475c | ACS Catal. 2012, 2, 2100−2113

fraction is *cis*-2-butene), even at low diene conversions (<3%), two explanations are suggested: (a) the presence of acidic sites at the aluminum centers of the zeolite, adjacent to the rhodium complexes, modifies the mode of addition of hydrogen to 1,3-butadiene in favor of the 1,4 addition[3,48,49] or (b) 1-butene formed from 1,3-butadiene desorbs from the rhodium sites after a 1,2-hydrogen addition (as observed for the MgO catalyst) and readsorbs on a distant acidic site within the porous zeolite to undergo isomerization before release into the gas stream. However, we stress that isomerization of 1-butene on acidic zeolites typically yields the most thermodynamically stable *trans*-2-butene, and not *cis*-2-butene, as the major isomer.[51] Thus, the comparison suggests that our catalyst operates differently from the one stated in postulate b. Moreover, the fact that, according to our data (Figure 2), no isomerization of the alkene takes place via secondary reactions suggests that readsorption of the various *n*-butene conformers on the acidic sites of the zeolite is kinetically insignificant.

The mode of catalytic action suggested in theory a, in contrast, is in good agreement with the observation that each single rhodium complex on the zeolite is isolated atop an aluminum site, as evidenced by IR and EXAFS spectra (Figure 1 and Table 1) (consistent with earlier reports[13,47]), and is also in good agreement with the dual reaction mechanism proposed for the dimerization of ethylene to give *n*-butenes with the same catalyst,[47] whereby the presence of the surface acidic site adjacent to the metal center is responsible for altering the mode of adsorption of the alkene, with the two types of active sites working in concert for the formation of the new C−C bond, as depicted above.

Remarkably, as one would anticipate on the basis of the reported observations of ethylene dimerization,[47] demonstrating that the activation of C═C bonds by the acidic surface sites is strongly hindered when the catalyst incorporates rhodium clusters that supply larger amounts of activated hydrogen (via spillover)[34] to the catalyst surface (which shifts the equilibrium of adsorption Al−OH + C_2H_4 ↔ Al−OH−C_2H_4 to the left),[47] we observed that the selectivity for formation of *cis*-2-butene in the hydrogenation of 1,3-butadiene drops markedly (from ∼65% to ∼25%) as the rhodium complexes are transformed into small clusters.

Hydrogenation of 1,3-Butadiene: Influence of CO Ligands on Essentially Molecular Rhodium Species. Prompted by the realization that the catalytic performance of rhodium for the partial hydrogenation of 1,3-butadiene is subject to fine-tuning when the catalytic species are essentially molecular in character, we sought to modify the catalytic sites by incorporation of ligands bonded to the rhodium, following a strategy that is typical in organometallic solution catalysis.[52,53] We selected CO, which facilely replaces ethylene in rhodium complexes and ethyl in rhodium clusters,[17] because CO is a ligand known to inhibit H_2 dissociation on extended metal surfaces.[44,54] Indeed, the use of CO cofed with 1,3-butadiene streams has been shown to increase the selectivity to butenes when conventional supported (nonmolecular) palladium catalysts are used,[44] but significantly, in our case (Table 2), the effect of CO on the catalytic performance of rhodium (as a ligand that can be precisely characterized, and not an ill-defined surface modifier) is strongly dependent on the structure of the rhodium species, and our results show a strong benefit of the CO only when the rhodium is present in clusters on an electron-donor support, evidently to induce the desired hydrogenation selectivity. Contacting of the MgO-supported rhodium complex with CO led to the formation of rhodium *gem*-dicarbonyls (Figure 1) and to complete deactivation of the catalyst for 1,3-butadiene hydrogenation (Table 2). This result is consistent with reports demonstrating that CO bonds strongly (almost irreversibly at 313 K and 1 bar in mixtures of H_2 and alkenes) to the mononuclear rhodium complexes when the support acts as an electron-donating ligand, hindering the activation of other species, such as alkenes and H_2.[44,54]

In contrast, the isostructural $Rh(CO)_2$ species supported on the acidic, weakly electron-donating HY zeolite has been found to be the precursor of a catalyst that is active for the 1,3-butadiene hydrogenation, although at rates lower than those observed with the complexes initially present as $Rh(C_2H_4)_2$ on the same support (Table 2). As was recently demonstrated,[13,20] the high activity of the $Me(CO)_2$ species (Me = Rh or Ir) on the zeolite relative to that on MgO is attributed to an increase in the capacity of the active sites to coordinate reactants (alkene and hydrogen) as the metal becomes more electron-deficient on the electron-withdrawing support. This inference is bolstered by the observation that zeolite-supported $Rh(CO)_2$ complexes readily transform into $Rh(C_2H_4)(CO)$ in ethylene at 298 K and 1 bar,[55] whereas the isostructural $Rh(CO)_2$ species on MgO are stable under these conditions.[14]

The incorporation of CO into the zeolite-supported rhodium complexes led to a slight increase in the selectivity for formation of *n*-butenes (Table 2), following the trend observed with conventional palladium catalysts,[44] but in contrast to the observations with palladium, the improvement we observed with our rhodium catalyst was only modest (with the selectivity increasing from ∼92% to ∼95% at a conversion of 5%, whereas the increase was from ∼80% to ∼99% at high diene conversions with palladium). Thus, the data indicate that the performance of the zeolite-supported rhodium complexes incorporating CO was still less than would be desired.

In contrast, and surprisingly, when the supported rhodium was present as clusters rather than mononuclear complexes, the effect of CO on the selectivity was dramatic, but only when the support was MgO (recall that on the zeolite, the clusters in CO fragmented readily to give $Rh(CO)_2$ complexes). The incorporation of CO ligands in the MgO-supported rhodium dimers caused an almost complete suppression of any reaction leading to butane as a primary product, with selectivities to *n*-butenes being >99.5% at low 1,3-butadiene conversions (Figures 2 and 3B). Furthermore, the bonding of CO to the rhodium dimers also led to a marked decrease in the activity of the catalyst for H_2 activation, consistent with our earlier observation that the rate of H_2 dissociation must be inhibited to limit the formation of butane via primary reaction routes.

Most significantly for potential applications, the data (Figure 3B) show that the selectivity of the carbonylated rhodium dimers on MgO is high not only at low diene conversions, but even at conversions as high as 97%. This result indicates that the formation of butane as a secondary product is strongly hindered, too, a result that further differentiates our dimeric catalyst from other supported rhodium catalysts (which give butane as both primary and secondary product).[3,4]

To understand the effect of the carbonyl ligands on the catalyst performance, it is helpful to compare the product distributions observed with the MgO-supported dimers before and after exposure to CO. The selectivity for formation of *n*-butenes characterizing the CO-free rhodium dimers on MgO was nearly constant (75−80%) at diene conversions up to 80%,

but it dropped significantly (to ∼49%) as the conversion increased from 80 to 97% (Figure 3A).

In contrast, when CO ligands were present on the rhodium dimers, they gave exclusively *n*-butenes over a diene conversion range from 1 to 97% (Figure 3A). These results demonstrate that CO on the rhodium is critical to preventing the formation of butane at low diene conversions and, beyond that, even in sharply limiting hydrogenation of the *n*-butene products when the diene conversion exceeds ∼80%.

The CO ligands on the rhodium dimers also affected the conversion of the diene and the distribution of *n*-butene isomers in the product (Figure 3). The ratio of 1-butene to 2-butenes in the product decreased at conversions exceeding 80% when the catalyst was supported on MgO, when butane was formed in secondary reactions. Indeed, as shown in Figure 3A, butane formed in these secondary reactions exclusively from the terminal alkene, with the concentration of the other two isomers remaining nearly unchanged; they were not converted significantly. According to this picture, we postulate that 1-butene was the only isomer that readsorbed significantly on the CO-free active sites in competition with 1,3-butadiene, and 1-butene then could undergo complete hydrogenation to butane, but not further isomerization to *cis*- or *trans*-2-butene.

In contrast, the observations that on the MgO-supported carbonylated rhodium dimers (at conversions up to 97%) (a) butane was barely formed and (b) the distribution of *n*-butene isomers was essentially constant (∼53% 1-butene, ∼38% *trans*-2-butene, and ∼9% *cis*-2-butene) show that none of the monoalkenes readsorbed significantly on the active sites when even only small amounts of 1,3-butadiene were present in the reactant gas.

Taken together, the results indicate that CO strongly influences the performance of the supported rhodium dimers, inhibiting the formation of butane by both primary and secondary reactions, but it does not affect the rates of interconversion of butene isomers.

Moreover, our results show that with the MgO-supported carbonylated rhodium dimers when the 1,3-butadiene conversion exceeded about 97%, the selectivity to *n*-butenes dropped sharply, just as the distribution of the butene isomers began to change significantly (with the *cis*- and *trans*-conformers predominating, Figure 3B), an indication that the monoalkenes reacted further because they underwent significant readsorption on the catalyst, followed by hydrogenation and isomerization once the diene had been largely consumed. The marked changes in catalytic selectivity just as the diene was virtually depleted indicate preferential activation of 1,3-butadiene over the products of its reaction when the diene competes successfully for the catalytic sites. When there is too little diene, the butenes compete successfully for these sites, with the concomitant change in selectivity.

The importance of competitive adsorption phenomena in controlling the selectivities of solid catalysts has been widely demonstrated.[56−58] For example, platinum nanoparticles decorated with TiO_x species, which hydrogenate styrene faster than nitrobenzene when they react separately, selectively reduce the latter in styrene/nitrobenzene mixtures, even when the C═C/−NO_2 ratio is high.[56] In 1,3-butadiene hydrogenation, the adsorption modes of the diene and the butenes play an important role in the selectivity of palladium, platinum, and rhodium catalysts, as summarized above.[2−5,41,48] Accordingly, we suggest that the presence of CO ligands on the MgO-supported rhodium dimers modifies the mode of adsorption of the competing reactants to favor the selective catalyst performance reported here.

Hydrogenation of 1,3-Butadiene: Changes in Catalytic Performance Induced by Changes in Structure of Active Sites During Catalysis. Figures 4, 5, and SI S6 show that the performance of some of our catalysts changed during operation. Such an observation is typical in supported metal catalysis, as a large number of competing phenomena can occur. These may be chemical (e.g., poisoning with impurities in the feed[59]), physical (e.g., formation of carbonaceous deposits, leading to mass transfer limitations or blocking of catalytic sites[60,61]), or thermal (e.g., sintering of the metal species[62,63]).

Phenomena such as these are often challenging to elucidate for typical industrial catalysts, which are highly nonuniform. In contrast, our catalysts incorporate structurally simple and uniform active species that can be characterized incisively during catalysis, an advantage for the elucidation of the chemistry. For example, the MgO-supported rhodium dimers that incorporate CO ligands, which catalyze the hydrogenation of 1,3-butadiene with selectivities >99% at 97% conversion, showed increasing catalytic activities with time on stream, with conversions (at constant temperature, pressure, and flow rates of the reactants) ranging from 1% immediately after the feed flow started to 100% after several hours (Figure 5A), and when the conversion had increased to 97%, the selectivity to *n*-butenes dropped.

EXAFS data characterizing this catalyst before and after reaction indicate that the nuclearity of the sites remained essentially unchanged upon exposure to the H_2/1,3-butadiene stream (two Rh atoms, on average, per supported species), but the number of CO ligands bonded to each Rh atom decreased from ∼4 to ∼2, on average (Table 1) (the Rh−O coordination number characterizing the interaction of the rhodium with the support remained essentially constant, indicating, with the nearly constant Rh−Rh coordination number, that the cluster size did not change substantially). These results emphasize the stability of the dimeric species on the MgO and show that some of the CO ligands were removed during operation of the catalyst.

Decarbonylation of the rhodium species during catalysis was confirmed by the IR spectra (Figure 5B) of the working catalyst. In flowing mixtures of H_2 and 1,3-butadiene at 313 K and 1 bar, the IR spectra show a gradual decrease in the intensity of the ν_{CO} bands at 2025, 1958, 1893, and 1853 cm^{-1} (the first two assigned to terminal carbonyls and the others to carbonyl ligands bridging two Rh atoms) and a less significant increase in intensity of the bands at 2001 and 2074 cm^{-1}, both assigned to terminally bonded CO ligands.[15] The total area under these carbonyl peaks decreased with time on stream, demonstrating decarbonylation. These changes in the IR spectra occurred as the activity for 1,3-butadiene hydrogenation was increasing (Figure 5A). The fact that the final dimeric structures, after attainment of apparently steady-state IR band intensities, incorporated exclusively terminal carbonyl ligands (Figure 5B), is in agreement with the observation that bridging CO ligands are usually less stable than terminal CO ligands.[64]

Taken together, the EXAFS results, showing a Rh−CO coordination number of ∼2 after reaction, and the final IR spectra showing the presence of only two intense bands in the ν_{CO} region, at 2074 and 2001 cm^{-1}, suggest the formation of $(CO)_2Rh{-}Rh(CO)_2$ species on the MgO. We emphasize, however, that additional ligands such as alkyl or hydride,

dx.doi.org/10.1021/cs300475c | ACS Catal. 2012, 2, 2100−2113

expected intermediates in the hydrogenation of 1,3-butadiene,[65,66] were likely bonded to the rhodium.[67]

A plot of the total area under the carbonyl peaks vs time shows a decrease consistent with the increase in the formation of butenes (as determined by mass spectrometry) vs time on stream (SI Figure S10). Thus, we infer that the decarbonylation led to an increase in the catalytic activity, and we suggest the following interpretation:

Immediately after the injection of the CO pulse (prior to the start of catalytic reaction), the MgO-supported species approximated as $Rh_2(CO)_6$, in which rhodium is expected to be zerovalent,[68] are expected to have been coordinatively saturated, with each Rh atom being an 18-e^- species (9 e^- provided by Rh^0; 4 by the two terminal carbonyl ligands; 2 by the two bridging carbonyl ligands; 2 by one oxygen atom of the support; and 1 by the Rh−Rh bond), which accounts for the lack of activity for catalytic hydrogenation of 1,3-butadiene at time on stream = 0. As decarbonylation took place, coordinatively unsaturated rhodium species formed, enabling the activation of 1,3-butadiene and H_2 that resulted in catalytic activity. For example, the final species approximated as $Rh_2(CO)_4$ presumably consisted of two Rh atoms that are 16-e^- species (9 e^- provided by Rh^0; 4 by the two terminal carbonyl ligands; 2 by one oxygen atom of the support; and 1 by the Rh−Rh bond) so that the catalytic unit was able to take on both the activation of one of the C═C bonds of 1,3-butadiene and the activation of H_2 to generate rhodium hydride species. We stress that these $Rh_2(CO)_4$ species are different from mononuclear rhodium *gem*-dicarbonyl species on the same support, also inferred to be 16-e^- species (8 e^- provided by Rh^+, 4 by the two terminal carbonyl ligands, and 4 by the two oxygen atoms of the support), but barely active for the hydrogenation of 1,3-butadiene, because the dimeric species include two 16-e^- rhodium species that work in tandem to take on the separate functions during catalysis (bonding of alkene, activation of H_2). This explanation accounts for the higher hydrogenation activity of the dimeric species[46] (Table 2).

Following this interpretation, we offer the following insights into the action of other catalysts investigated here. For example, the slight increase in catalytic activity with time on stream observed for the MgO-supported $Rh(C_2H_4)_2$ species (Figure 4) can be ascribed to an incipient transformation of the mononuclear complexes into clusters, more active for hydrogenation than the mononuclear rhodium complexes, as illustrated in Table 2. This process is evidenced by the IR spectra of the sample probed with CO after several hours of reaction, which demonstrates the appearance of two weak, broad bands, at 1853 and 1893 cm^{-1} (data not shown), assigned to bridging CO ligands in the rhodium clusters. (The intensities of these bands are much lower than those characterizing the sample in which the rhodium was essentially all in the form of dimers (Figure 1A).)

In contrast, the catalyst initially incorporating $Rh(C_2H_4)_2$ complexes on the zeolite showed a decreasing activity with time on stream in the flow reactor (Figure 4). There is no evidence of the formation of rhodium clusters in this case. Instead of an activation mechanism, a deactivation mechanism was evidently in play. The decay in the hydrogenation activity of the zeolite-supported rhodium complex with time on stream was accompanied by a massive accumulation of hydrocarbons on the catalyst surface, as evidenced by IR spectra recorded after purging of the gas-phase reactants with flowing helium and showing a marked increase in the intensity of bands in the C−H stretching region after 1 h of reaction, as shown in SI Figure S7B. By analogy with the mode of action of these zeolite-supported rhodium complexes initially present as $Rh(C_2H_4)_2$ in the dimerization of ethylene to *n*-butenes, the gradual accumulation of surface hydrocarbons (presumably polymers) evidently caused deactivation of the catalyst as the active sites were poisoned with strongly adsorbed species or as the access of the reactants to the catalytic sites was hindered.[47] Moreover, the decrease in the TOF values with time on stream with this sample was accompanied by a decrease in the selectivity of the catalyst for formation of *n*-butenes (SI Figure S6). On the basis of the inference that the observed accumulation of hydrocarbons on the catalyst indicates a limitation of the desorption of the reaction products, we postulate that the increase in selectivity to butane resulted from the longer contact times between the *n*-butene intermediates and the active sites as the catalyst underwent deactivation, favoring the conversion of a larger fraction of the adsorbed species into fully hydrogenated products before release from the surface.

CONCLUSIONS

The performance of rhodium in the form of mononuclear complexes and extremely small clusters on either an electron-donor support, MgO, or a weaker electron-donor support, HY zeolite, incorporating relatively reactive ethylene or ethyl ligands or deactivating CO ligands was investigated for the catalytic hydrogenation of 1,3-butadiene and for the catalytic reaction of H_2 with D_2 to form HD. Starting from $Rh(C_2H_4)_2$ complexes on each support, treatment with H_2 at 353 K and 1 bar led to the formation of rhodium clusters that are larger on the zeolite surface (∼4 Rh atoms per catalytic unit, on average, versus 2 Rh atoms on MgO), as indicated by EXAFS and IR spectra. These subtle changes in metal nuclearity, from 1 to 2 to 4, lead to marked changes in the catalytic selectivity for *n*-butenes at low conversions of 1,3-butadiene (<15%), provided that CO is not present to poison the sites. The formation of butane as a primary product correlates well with the rate at which each catalyst dissociates H_2, as inferred from the catalytic H−D exchange results, with the exception of the zeolite-supported mononuclear rhodium complexes, which, notwithstanding the fast activation of H_2, produce *n*-butenes with relatively high selectivities. The dual metal−acid function of the zeolite-supported catalyst, moreover, is responsible for alteration of the distribution of the *n*-butene isomers, with *cis*-2-butene being the most abundant isomer when the support is acidic, but with 1-butene dominating when the support is the basic MgO (and we stress that *trans*-2-butene is thermodynamically favored). Although the behavior of the catalysts is largely affected by the nuclearity of the rhodium species and the support as a macroligand, our results indicate that the selectivity to butenes cannot be optimized just by controlling these two properties. However, all the catalytic routes that yield butane as a product are suppressed when the catalyst is in the form of rhodium dimers on MgO and when they are selectively poisoned with CO. In these structures, the carbonyl ligands in bridging positions on the metal frame are easily replaced by 1,3-butadiene and H_2 to undergo a reaction in which the rate of H_2 dissociation is properly mitigated to avoid formation of butane via primary routes, and the adsorption mode of the diene is evidently altered to favor its preferential activation, even in the presence of an excess of *n*-butenes, opening the way to selectivities to butenes as high as the best reported with gold catalysts, but under much milder reaction conditions.

dx.doi.org/10.1021/cs300475c | ACS Catal. 2012, 2, 2100−2113

EXPERIMENTAL SECTION

Materials, Sample Preparation, and Handling. Sample synthesis and handling were performed with the exclusion of air and moisture by use of standard Schlenk techniques and a glovebox purged with argon that was circulated through traps containing supported copper and zeolite 4A for removal of O_2 and moisture, respectively. Prior to adsorption of the precursor $Rh(C_2H_4)_2(acac)$ on MgO or zeolite HY, these supports were treated as follows: The MgO powder support (EM Science, surface area ~70 m^2 g^{-1}) was treated with deionized water to form a paste, which was dried in air at 393 K. The solid was ground and calcined by heating in flowing O_2 from room temperature to 973 K at a rate of 3 K/min, then held at this temperature for 2 h. The O_2 treatment was followed by evacuation of the support at 1.33×10^{-3} mbar for 14 h at 973 K, then cooling to room temperature. Zeolite HY (Zeolyst International, Conshohocken, NJ) was calcined by heating in flowing O_2 from room temperature to 773 K at a rate of 3 K/min, then held for 2 h. The O_2 treatment was followed by evacuation at 1.33×10^{-3} mbar for 14 h at 773 K, followed by cooling to room temperature. The supported rhodium complex was prepared by bringing the precursor $Rh(C_2H_4)_2(acac)$ (Strem, 99%) into contact with the calcined MgO or zeolite HY support in a slurry with *n*-pentane (Fisher, 99%) for 24 h; the solvent was removed by evacuation for 24 h. The resultant catalysts, which contained 0.4 wt % and 1 wt % Rh on MgO and zeolite HY, respectively, were stored in the glovebox. Reduction of each of the catalysts was performed at 353 K with H_2 flowing at 50 mL(NTP)/min.

Helium (Airgas, 99.999%), H_2 (Praxair, 99.999%), CO (Airgas, 10% balanced with helium), and 1,3-butadiene (Airgas, 2 vol % balanced with H_2) were purified by passage through traps containing supported copper and zeolite 4A to remove traces of O_2 and moisture, respectively.

Infrared Spectroscopy. A Bruker IFS 66v/S spectrometer with a spectral resolution of 2 cm^{-1} was used to collect transmission IR spectra of MgO or zeolite HY-supported rhodium samples. In the argon-filled glovebox, each sample (typically, 50 mg), handled with exclusion of air and moisture, was pressed into a thin wafer and loaded into the cell (In-situ Research Institute, South Bend, IN) through which gases flowed. The cell was connected to a vacuum system with a base pressure of 1.33×10^{-3} mbar that allowed recording of spectra while reactant gases (H_2, CO, and/or 1,3-butadiene) flowed through the cell at a temperature in the range of 298−353 K. Spectra were collected in the mid-IR region with a deuterated triglycine sulfate (DTGS) detector. Each spectrum represents the average of 64 scans.

Mass Spectrometry. Mass spectra of the effluent gases introduced into the flow system or produced by reaction with the sample were measured with an online Balzers OmniStar mass spectrometer running in multi-ion monitoring mode; these data were collected as IR spectra were being recorded. Changes in the intensities of major fragments of C_4H_8 (m/e = 39, 41, and 56) and C_4H_{10} (m/e = 29 and 43) were recorded.

X-ray Absorption Spectroscopy. X-ray absorption spectra were recorded at X-ray beamline 4-1 at the Stanford Synchrotron Radiation Lightsource. The storage ring electron energy was 3.0 GeV. The cryogenic double-crystal silicon (Si(220)) monochromator was detuned by 15−20% at the Rh K edge to minimize the effects of higher harmonics in the X-ray beam. Powder samples were pressed into self-supporting wafers in a nitrogen-filled glovebox. Each wafer was loaded into a flow-through cell for time-resolved experiments or an EXAFS cell that was evacuated to a pressure of 1.33×10^{-5} mbar for steady-state experiments. Spectra of the samples were collected in transmission mode, and a reference rhodium foil was scanned simultaneously with the samples. The mass of each sample wafer was ~0.6 g, calculated to give an optimal X-ray absorbance of 2.5 at the Rh K edge (23220 eV). For steady-state experiments, each sample was scanned at liquid-nitrogen temperature, and four scans were recorded per sample. For time-resolved experiments, each sample was scanned at 298 K in the presence of helium for 1 h and then as the sample was treated in flowing H_2 for 20 min as the temperature was ramped from 298 to 353 K and further as the sample was held at 353 K in flowing H_2 for another hour. The flow rates of helium and of H_2 were 50 mL/min. XANES and EXAFS spectra were recorded at intervals of 2 and 15 min, respectively.

EXAFS Data Analysis. Two consecutive spectra were averaged for the analysis of time-resolved EXAFS data. The EXAFS data analysis was carried out with the software ATHENA of the IFEFFIT package and with the software XDAP.[69,70] Reference files were used for phase shifts and backscattering amplitudes that were calculated by using the code FEFF 7.0.[71] Rhodium foil was used as a standard for Rh−Rh contributions;[72] experimental XRD results characterizing $Rh(C_2H_4)_2(acac)$ were used for Rh−C and Rh−O contributions.[73] A Rh−Mg reference file was calculated with structural parameters representing the compound Rh_2MgO_4, and a Rh−Al reference file was calculated for Rh−Al alloy.[74] Reference files for rhodium carbonyl contributions were calculated from structural parameters representing $Rh(CO)_2(acac)$.

The X-ray absorption edge energy is defined as the inflection point of the first absorption peak at the Rh K edge (23 220 eV), which was calibrated by scanning a rhodium foil simultaneously with the sample. XDAP was used for edge calibration, deglitching, data normalization (calculated by dividing the absorption intensity by the height of the absorption edge), and background subtraction. XDAP allowed a "difference-file" technique[75,76] to determine optimized parameters for individual shell contributions. Iterative fitting was carried out until good agreement was achieved between the calculated k^1- and k^3-weighted EXAFS data and the postulated model. The approximate accuracies of the fit parameters characterizing the absorber−backscatterer pair contributions are estimated to be as follows: coordination number N, ±20%; distance R, ±0.02% Å; disorder term $\Delta\sigma^2$, ±20%; and inner potential correction ΔE_0, ±20%. The number of parameters used in the fitting was always less than the statistically justified number, computed with the Nyquist theorem:[77] $n = (2\Delta k \Delta r/\pi) + 2$, where Δk and Δr, respectively, are the k and r (distance) ranges of the data used in the fitting. Details of the fitting and plots are included in the Supporting Information.

Catalytic Reaction Experiments. Hydrogenation of 1,3-butadiene was carried out in a nearly isothermal, once-through reactor (well approximated as a plug-flow reactor), which was a quartz tube with an internal diameter of 0.8 cm fitted with a quartz frit. Reactions were carried out at temperatures in the range of 298−333 K and atmospheric pressure (total gas feed flow rate, 30 mL NTP/min; feed component partial pressures, 20 mbar of C_4H_6, 980 mbar of H_2). The typical catalyst with a mass usually in the range of 5.00−200 mg was diluted with particles of inert, nonporous α-Al_2O_3 in a mass ratio of 1:60, to give a bed of approximately 2.5 cm in length to prevent

dx.doi.org/10.1021/cs300475c | ACS Catal. 2012, 2, 2100−2113

channeling of the gas mixture. The catalyst was loaded into the reactor in a glovebox and installed in the flow system without exposure to air and moisture. The reaction conditions were chosen to give differential conversions ($0 < X < 10\%$) to allow a comparison of TOF values representing the various catalysts. Products were analyzed by gas chromatography with an HP-6890 instrument equipped with a 50 m × 0.53 mm PLOT Alumina "M" capillary column (J & W Scientific) and a flame-ionization detector. The product stream was sampled every 12 min for analysis. Conversions and selectivities were determined from the GC areas corresponding to the reactant (1,3-butadiene) and products (butane, 1-butene, *trans*-2-butene, and *cis*-2-butene).

■ ASSOCIATED CONTENT

Supporting Information

Additional information as noted in text. This material is available free of charge via the Internet at http://pubs.acs.org.

■ AUTHOR INFORMATION

Corresponding Author

*E-mails: (B.C.G.) bcgates@ucdavis.edu, (P.S.) psername@itq.upv.es.

Notes

The authors declare no competing financial interest.

■ ACKNOWLEDGMENTS

We thank the DOE Division of Materials Sciences for its role in the operation and development of beamline 4-1 at the Stanford Synchrotron Radiation Lightsource. We thank the beamline staff for valuable support. The research was supported by the European Union Seventh Framework Programme (FP7/2007-2013) under grant agreement PIOF-GA-2009-253129 (P.S.) and by DOE Basic Energy Sciences (Contract No. FG02-04ER15513) (D.Y.).

■ REFERENCES

(1) Zhang, X.; Xamena, F. X. L.; Corma, A. *J. Catal.* **2009**, *265*, 155.
(2) Tourillon, G.; Cassuto, A.; Jugnet, Y.; Massardie, J.; Bertolini, J. C. *J. Chem. Soc., Faraday Trans.* **1996**, *92* (23), 4835.
(3) Boitiaux, J. P.; Cosyns, J.; Robert, E. *Appl. Catal.* **1987**, *35*, 193.
(4) Bond, G. C.; Webb, G.; Wells, P. B.; Winterbottom, J. M. *J. Chem. Soc.* **1965**, *0*, 3218.
(5) Valcarcel, A.; Clotet, A.; Ricart, J. M.; Delbecq, F.; Sautet, P. *Surf. Sci.* **2004**, *549*, 121.
(6) Comas-Vives, A.; Gonzalez-Arellano, C.; Corma, A.; Iglesias, M.; Sanchez, F.; Ujaque, G. *J. Am. Chem. Soc.* **2006**, *128*, 4756.
(7) Guzman, J.; Gates, B. C. *Angew. Chem., Int. Ed.* **2003**, *42*, 690.
(8) Hugon, A.; Delannoy, L.; Louis, C. *Gold Bull.* **2008**, *41/2*, 127.
(9) Herrmann, W. A.; Frey, G. D.; Herdtweck, E.; Steinbeck, M. *Adv. Synth. Catal.* **2007**, *349*, 1677.
(10) Timmer, K.; Thewissen, D. H. M. W.; Meinema, H. A.; Bulten, E. J. *Rec. Trav. Chim. Pays-Bas* **1990**, *109*, 87.
(11) Zahmakıran, M.; Román-Leshkov, Y.; Zhang, Y. *Langmuir* **2012**, *28* (1), 60.
(12) Argo, A. M.; Odzak, J. F.; Goellner, J. F.; Lai, F. S.; Xiao, F.-S.; Gates, B. C. *J. Phys. Chem. B* **2006**, *110*, 1775.
(13) Liang, A. J.; Bhirud, V. A.; Ehresmann, J. O.; Kletnieks, P. W.; Haw, J. F.; Gates, B. C. *J. Phys. Chem. B* **2005**, *109*, 24236.
(14) Ogino, I.; Gates, B. C. *J. Am. Chem. Soc.* **2008**, *130*, 13338.
(15) Bhirud, V. A.; Ehresmann, J. O.; Kletnieks, P. W.; Haw, J. F.; Gates, B. C. *Langmuir* **2006**, *22*, 490.
(16) Liang, A. J.; Gates, B. C. *J. Phys. Chem. C* **2008**, *112*, 18039.
(17) Serna, P.; Gates, B. C. *J. Am. Chem. Soc.* **2011**, *133*, 4714.
(18) Yardimci, D.; Serna, P.; Gates, B. C. *ChemCatChem*, **2012**, DOI: 10.1002/cctc.201200033.
(19) Wang, Q.; Hanson, J. C.; Frenkel, A. I. *J. Chem. Phys.* **2008**, *129*, 234502.
(20) Lu, J.; Serna, P.; Gates, B. C. *ACS Catal.* **2011**, *1*, 1549.
(21) Allian, A. D.; Wang, Y.; Saeys, M.; Kuramshina, G. M.; Garland, M. *Vib. Spectrosc.* **2006**, *41*, 101.
(22) Chenier, J. H. B.; Histed, M.; Howard, J. A.; Joly, H. A.; Morris, H.; Mile, B. *Inorg. Chem.* **1989**, *28*, 14.
(23) Hanlan, L. A.; Ozin, G. A. *J. Am. Chem. Soc.* **1974**, *96*, 6324.
(24) Kawi, S.; Xu, Z.; Gates, B. C. *Inorg. Chem.* **1994**, *33*, 503.
(25) Cariati, E.; Dragonetti, C.; Roberto, D.; Ugo, R.; Lucenti, E. *Inorg. Chim. Acta* **2003**, *349*, 189.
(26) Feng, X.; Xie, C.; Liu, Z.; Xie, Y.; King, R. B.; Schaefer, H. F., III *Dalton Trans.* **2009**, *14*, 2599.
(27) The spectra of the zeolite in the absence of rhodium include a broad band centered at 1870 cm^{-1}. After adsorption of the $Rh(C_2H_4)_2(acac)$, treatment of the resulting sample with flowing H_2 at 353 K and 1 bar for 1 h, and subsequent contact of the sample with a pulse of CO in helium at 298 K and 1 bar, a small shoulder appeared at 1830 cm^{-1} (Figure 1B, inset).
(28) Huttner, G.; Knoll, K. *Angew. Chem., Int. Ed.* **1987**, *26*, 743.
(29) Suzuki, A.; Inada, Y.; Yamaguchi, A.; Chihara, T.; Yuasa, M.; Nomura, M.; Iwasawa, Y. *Angew. Chem.* **2003**, *115*, 4943.
(30) Berkó, A.; Solymosi, F. *J. Catal.* **1999**, *183*, 91.
(31) Bergeret, G.; Gallezot, P.; Gelin, P.; Ben Taarit, Y.; Lefebvre, F.; Naccache, C.; Shannon, R. D. *J. Catal.* **1987**, *104*, 279.
(32) Wong, T. T. T.; Stakheev, A. Y.; Sachtler, W. M. H. *J. Phys. Chem.* **1992**, *96*, 7733.
(33) Bhore, N. A.; Klein, M. T.; Bischoff, K. B. *Ind. Eng. Chem. Res.* **1990**, *29*, 313.
(34) Conner, W. C.; Falconer, J. L. *Chem. Rev.* **1995**, *95*, 759.
(35) Al-Ammar, A. S.; Webb, G. *J. Chem. Soc. Faraday Trans.* **1979**, *175*, 1900.
(36) Grunes, J.; Zhu, J.; Yang, M.; Somorjai, G. A. *Catal. Lett.* **2003**, *86*, 157.
(37) Alayoglu, S.; Nilekar, A. U.; Mavrikakis, M.; Eichhorn, B. *Nat. Mater.* **2008**, *7*, 333.
(38) Voge, H. H.; May, N. C. *J. Am. Chem. Soc.* **1946**, *68*, 550.
(39) Houžvička, J.; Ponec, V. *Catal. Rev.: Sci. Eng.* **1997**, *39*, 319.
(40) Seth, D.; Sarkar, A.; Ng, F. T. T.; Rempel, G. L. *Chem. Eng. Sci.* **2007**, *62*, 4544.
(41) Piccolo, L.; Piednoir, A.; Bertolini, J.-C. *Surf. Sci.* **2005**, *592*, 169−181.
(42) Furlong, B. K.; Hightower, J. W.; Chan, T.-Y.-L.; Sarkany, A.; Guczi, L. *Appl. Catal., A* **1994**, *117*, 41.
(43) Umpierre, A. P.; Machado, G.; Fecher, G. H.; Morais, J.; Dupont, J. *Adv. Synth. Catal.* **2005**, *347*, 1404.
(44) Silvestre-Albero, J.; Rupprechter, G.; Freund, H.-J. *J. Catal.* **2005**, *235*, 52.
(45) Gross, A. *Appl. Phys. A: Mater. Sci. Process.* **1998**, *67*, 627.
(46) Lu, J.; Serna, P.; Aydin, C.; Browning, N. D.; Gates, B. C. *J. Am. Chem. Soc.* **2011**, *133*, 16186.
(47) Serna, P.; Gates, B. C. *Angew. Chem., Int. Ed.* **2011**, *50*, 5528.
(48) Silvestre-Albero, J.; Rupprechter, G.; Freund, H.-J. *J. Catal.* **2006**, *240*, 58.
(49) Bertolini, J. C.; Cassuto, A.; Jugnet, Y.; Massardier, J.; Tardy, B.; Tourillon, G. *Surf. Sci.* **1996**, *349*, 88.
(50) Aguayo, A. T.; Arandes, J. M.; Olazar, M.; Bilbao, J. *Ind. Eng. Chem. Res.* **1990**, *29*, 1172.
(51) Kondo, J. N.; Domen, K. *J. Mol. Catal. A: Chem.* **2003**, *199*, 27.
(52) Cotton, F. A.; Wilkinson, G. *Advanced Inorganic Chemistry*, Wiley-Interscience, New York, 1967.
(53) Crabtree, R. H. *The Organometallic Chemistry of the Transition Metals*, 4th ed.; Wiley: New York, 2005.
(54) Basu, P.; Yates, J. T., Jr. *J. Phys. Chem.* **1989**, *93*, 6110.
(55) Liang, A. J.; Craciun, R.; Chen, M.; Kelly, T. G.; Kletnieks, P. W.; Haw, J. F.; Dixon, D. A.; Gates, B. C. *J. Am. Chem. Soc.* **2009**, *131*, 8460.

(56) Corma, A.; Serna, P.; Concepción, P.; Calvino, J. J. *J. Am. Chem. Soc.* **2008**, *130*, 8748.
(57) Lee, D. C.; Kim, J. H.; Kim, W. J.; Kang, J. H.; Moon, S. H. *Appl. Catal., A* **2003**, *244*, 83.
(58) Boronat, M.; Concepción, P.; Corma, A.; González, S.; Illas, F.; Serna, P. *J. Am. Chem. Soc.* **2007**, *129*, 16230.
(59) Rodriguez, J. C.; Romeo, E.; Fierro, J. L. G.; Santamaria, J.; Monzon, A. *Catal. Today* **1997**, *37*, 255.
(60) Kelly, D. G.; Odriozola, J. A.; Somorjai, G. A. *J. Phys. Chem.* **1987**, *91*, 5695.
(61) Oudar, J.; Pinol, S.; Berthier, A. *J. Catal.* **1987**, *107*, 434.
(62) Kim, W. J.; Kang, J. H.; Ahn, I. Y.; Moon, S. H. *J. Catal.* **2004**, *226*, 226.
(63) Albers, P.; Pietsch, J.; Parker, S. F. *J. Mol. Catal. A: Chem.* **2001**, *173*, 275.
(64) Alexeev, O. S.; Panjabi, G.; Phillips, B. L.; Gates, B. C. *Langmuir* **2003**, *19*, 9494.
(65) Argo, A. M.; Odzak, J. F.; Lai, F. S.; Gates, B. C. *Nature* **2002**, *415*, 623.
(66) Muetterties, E. L.; Krause, M. J. *Angew. Chem., Int. Ed. Engl.* **1983**, *22*, 135.
(67) The spectra in the ν_{CH} region after reaction (once the gas-phase reactants had been purged with helium) included a set of bands corresponding to hydrocarbons that could either be bonded to the rhodium or weakly adsorbed on the support. Detection of these hydrocarbons by EXAFS spectroscopy is not feasible, being hindered by the limitation of the technique in differentiating light backscatterers at similar distances from the Rh atom and by the maximum number of parameters that can be realistically accounted for in a fit of the data (details in SI). Both IR and EXAFS spectroscopies are of limited value for the detection of hydrides in samples such as ours. Koningsberger, D. C.; Mojet, B. L.; van Dorssen, G. E.; Ramaker, D. E. *Top. Catal* **2000**, *10*, 143.
(68) Parkin, G. *Struct. Bonding (Berlin)* **2010**, *136*, 113.
(69) Newville, M.; Ravel, B.; Haskel, D.; Rehr, J. J.; Stern, E. A.; Yacoby, Y. *Physica B* **1995**, *208/209*, 154.
(70) Newville, M. J. *Synchrotron Radiat.* **2001**, *8*, 96.
(71) Zabinsky, S. I.; Rehr, J. J.; Ankudinov, A.; Albers, R. C.; Eller, M. J. *Phys. Rev. B* **1995**, *52*, 2995.
(72) Villars, P.; Calvert, L. D. *Pearson's Handbook of Crystallographic Data for Intermetallic Phases*; American Society for Metals: Metals Park, OH, 1985; Vol. 3; p 3090.
(73) Buhl, M.; Hakansson, M.; Mahmoudkhani, A. H.; Ohrstrom, L. *Organometallics* **2000**, *19*, 5589.
(74) Donnay, J. D. H.; Ondik, H. M. *Crystal Data Determinative Tables*; National Bureau of Standards and the Joint Committee on Powder Diffraction Standards, Washington, DC, 1973, Vol. *II*, p C-4.
(75) Kirlin, P. S.; van Zon, F. B. M.; Koningsberger, D. C.; Gates, B. C. *J. Phys. Chem.* **1990**, *94*, 8439.
(76) van Zon, J. B. A. D.; Koningsberger, D. C.; van't Blik, H. F. J.; Sayers, D. E. *J. Chem. Phys.* **1985**, *82*, 5742.
(77) Lytle, F. W.; Sayers, D. E.; Stern, E. A. *Physica B* **1989**, *158*, 701.